II International Conference on Particle-based Methods - Fundamentals and Applications
PARTICLES 2011
E. Oñate and D.R.J. Owen (Eds)

EFFECT OF PARTICLE SHAPE NON-CONVEXITY ON THE RHEOLOGY OF GRANULAR MEDIA: 3D CONTACT DYNAMICS SIMULATIONS

B. Saint-Cyr[*,†], E. Azéma[*], J.-Y. Delenne[*], F. Radjai[*] and P. Sornay[†]

[*]LMGC, CNRS-Université Montpellier 2, Montpellier, France.
Baptiste.saint-cyr@univ-montp2.fr

[†]CEA, DEN, SPUA, LCU, F-13108 St Paul lez Durance, France

Key words: Granular Materials, particle shape, non-convexity, texture, force transmission

Abstract. We analyze the effect of particle shape non-convexity on the quasi-static behavior of granular materials by means of contact dynamics simulations. The particles are regular aggregates of four overlapping spheres described by a nonconvexity parameter depending on the relative positions of the particles. Several packings are first submitted to isotropic compression without friction. We find that, as in 2D, the solid fraction of isotropic packings increases with non-convexity up to a maximum value and then declines to be nearly equal to that of a packing composed of only spheres. It is also remarkable that the coordination number increases quickly and saturates so that the packings composed of grains with a high level of nonconvexity are looser but more strongly connected. Then, the quasi-static behavior, structural and force anisotropies are analyzed by subjecting each packing to a triaxial compression. We find that the shear strength increases with non-convexity. We show that this increase results from the presence of multiple contacts between trimers leading to enhanced frictional interlocking.

1 INTRODUCTION

Spherical or circular shape have been mostly used to investigate the rheology and microstructure of granular materials. The widespread use of this idealized shape has been motivated by the fact that the rheology is mainly governed by the collective contact interactions of the particles. Nevertheless these models are not able to reflect some of the more complex aspects of real granular media behavior, such as high shear resistance observed for angular particles [3, 8, 9] or high volumetric changes in the case of elongated particles [5].

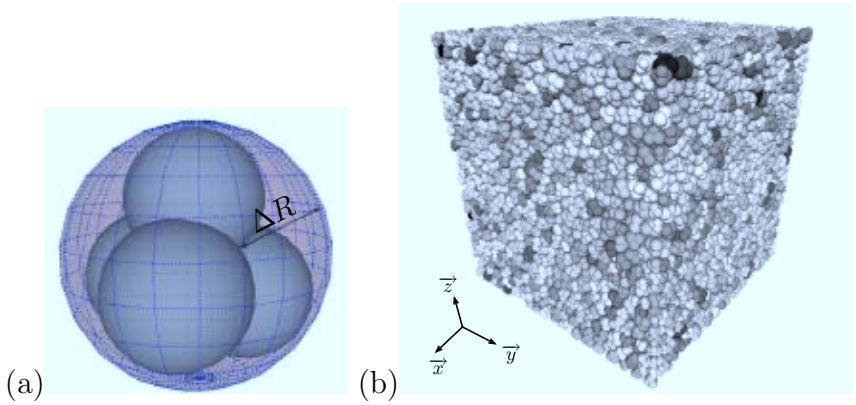

Figure 1: (a) Geometry of regular aggregate. (b) Map of particles pressure at the end of isotropic state for $\eta = 0.4$

Among the difficulties, except the fact that numerically the modeling of complex shape gives rise to various technical difficulties both geometrical and computational [6], is that 1) the shape parameters need to be defined conveniently in order to be able to generate particle shapes with continuously-variable shape parameters and 2) particle shape can be broken down into different categories: angular shape, non-convex shape, elongated shape...

In this work we focus more precisely on the effect of non-convexity on the rheology of granular media. We consider aggregates of four overlapped spheres as a 3D generalization of trimers [12] (aggregates of three overlapping disks in 2D). Our numerical approach is presented in Sec.2. We analyze the stress-strain behavior in sec.3 as well as the topology of the contact network and force transmission as a function of nonconvexity, respectively in sec.4 and 5.

2 NUMERICAL PROCEDURES

The shape of a regular aggregate composed of four spheres of radius r can be characterized by considering the radius R of the circumscribed sphere as compared to the radius R' of the inscribed sphere; Fig. 1(a). The difference $\Delta R = R - R'$ represents the concavity of the aggregate which, by definition, corresponds to the inward deviation from the surface of the circumscribed sphere. Hence, the non-convexity η can be defined by the ratio $\eta = \Delta R/R$. This parameter can be calculated as a function of the ratio $d/2r$, where d is the distance between the center of two spheres. This definition is similar to the so-called "Riley Sphericity" used to characterize thin sections in rock mechanic [7]. This parameter varies from 0, corresponding to a sphere, to $\eta \simeq 0.76$ corresponding to an aggregate where the constituting coplanar spheres intersect themselves at a single point (i.e. $d/2r = \sqrt{3}/2$).

We used contact dynamic (CD) simulations [1, 13, 10] to compact 12 000 aggregates (48 000 spheres) by isotropic compression inside a box of dimensions $L_0 \times l_0 \times H_0$ in

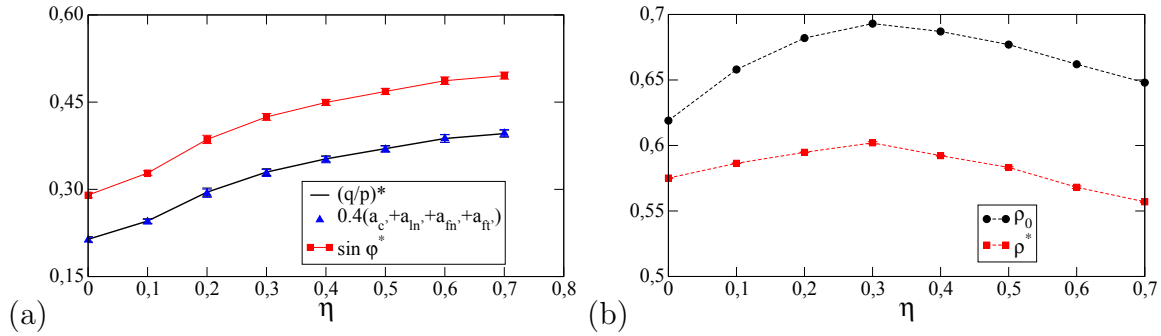

Figure 2: (a) Normalized shear stress $(q/p)^*$ averaged in the residual state together with the harmonic approximation and the friction angle $\sin\varphi$, (b) The initial and final solid fractions as a function of nonconvexity.

which the left, bottom and background walls are fixed and the top, the right and the front walls are subjected to the same compressive stress σ_0. The gravity and friction coefficients μ and μ_w between particles and with the walls, respectively, are set to zero in order to get homogeneous and isotropic dense packings. At equilibrium, all samples were in isotropic stress state. Eight samples are prepared according to this protocole for eight values of $\eta \in [0, 0.7]$. Figure 1(b) shows an example of packing obtain by this procedure for $\eta = 0.4$. The grey-level are proportional to the mean pressure. In order to avoid long-range ordering in the limit of small values of η, we introduce a size polydispersity by taking R in the range $[Rmin, 3Rmin]$ and a uniform distribution of particle volume fractions. These samples are then used as initial configuration for triaxial compression tests with $\mu = 0.4$ between particles. A downward velocity v_z is imposed on the upper wall while keeping a constant confining stress on lateral wall.

3 STRESS-STRAIN BEHAVIOR

The stress tensor $\boldsymbol{\sigma}$ can be evaluated from the simulation data as an average over all the contact of the dyadic product of contact force $\boldsymbol{f}^c$ and branch vector $\boldsymbol{\ell}^c$: $\sigma_{\alpha\beta} = n_c \langle f^c_\alpha \ell^c_\beta \rangle_c$ [1], where n_c is the number density of contacts c. Under triaxial conditions with vertical compression, we have $\sigma_1 \geq \sigma_2 = \sigma_3$, where the σ_α are the stress principal values. We extract the mean stress $p = (\sigma_1 + \sigma_2 + \sigma_3)/3$ and the stress deviator $q = (\sigma_1 - \sigma_3)/3$.

During shear, the shear stress jumps initially to a high value before decreasing to a nearly constant value in the steady state. The steady-state shear stress $(q/p)^*$ characterizes the shear strength of the material. According to the Mohr-Coulomb model, in triaxial geometry, the internal angle of friction, representing the shear strength of the material, is defined by $\sin\varphi^* = 3q/(2p+q)$ [7]. Figure 2(a) shows the variation of $(q/p)^*$ and $\sin\varphi^*$ averaged in the steady state as a function of η. We see that both $(q/p)^*$ and $\sin\varphi^*$ increases with η. We also observe that the prediction of an approximation from force and fabric anisotropies, to be discussed below, provides a nice fit to the simulation data.

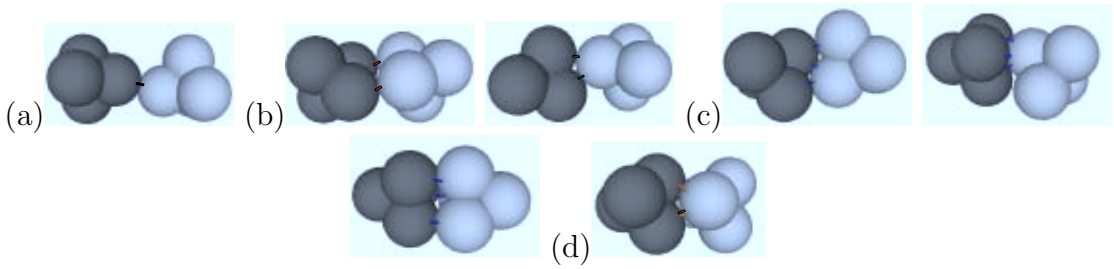

Figure 3: Different types of contact between two aggregate: (a) simple (s), (b) simple-double (sd) and double (d), (c) triple double-simple (tsd), double (td), simple (ts) and (d) quadruple contacts

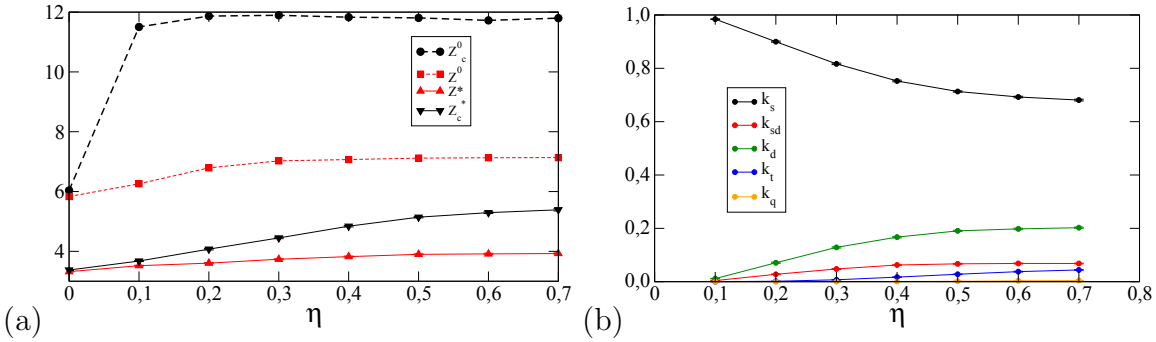

Figure 4: (a) Coordination Z and connectivity Z_c numbers as a function of η both at initial and residual state, (b) Proportion of k each contacts in the residual state as a function of η.

Figure 2(b) displays the solid fraction ρ at initial (isotropic) ρ^0 and critical ρ^* state as a function of non-convexity η. Interestingly, the solid fraction first grows in the range $\eta < 0.3$, then it declines slowly with η up to a value close to that for spheres for initial state and bellow to that of sheres for critical state. A similar unmonotonic behavior of packing fraction has been previously observed for granular packings of elongated particles such as ellipses, ellipsoidal particles, sphero-cylinders and rounded-cap rectangles [5, 11] . This is somewhat a counterintuitive finding as the shear strength (a monotonous function of η) does not follow the trend of solid fraction (non-monotonous).

4 CONTACT vs NEIGHBOR NETWORK

A major effect of concavities is to allow for multiple contacts between two aggregates. Various kinds of contacts can occur as shown in Fig3: (1) simple contact, (2) simple-double as two simple contacts between two pairs of spheres, or double contact, defined as two contacts between one sphere of one aggregate with two sphere of another aggregate, (3) triple contacts (t) defined as a combination of simple and double contacts (tsd), or one sphere of one aggregate and three spheres of other aggregate (td) or three simple contacts (ts), and (d) quadruple'(q) contacts as two times (2b) contacts. Note that, cinquple and sixtuple are possible but very rare, as well as td and ts contacts.

Thus, given multiple contacts between aggregates, we can distinguish between the

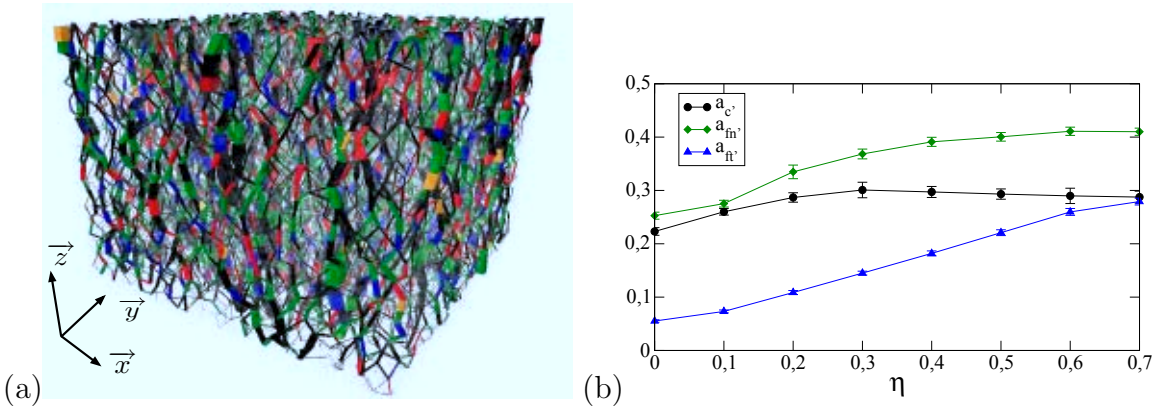

Figure 5: (a) Map of the neighbor force network at $\eta = 0.6$ Line thickness is proportional to the radial force. s-contacts are in black, sd-contacts in red, d-contacts are in green, t-contacts are in blue and q-contacts are in yellow. (b) branch, length-branch, radial and orthoradial force anisotropies averaged in the residual state as a function of η.

"coordination" number Z as the mean number of contact neighbors per particle (i.e. double, triple... contacts are seen as one contact), and the "connectivity" number Z_c defined as the mean number of contacts per particle.

Figure 4(a) plots Z and Z_c both in the isotropic and residual state as a function of η. We see that Z_c^0 jumps from 6 for spheres to $\simeq 12$ for $\eta > 0$. Indeed, this is compatible with the isostatic nature of our packings prepared with a zero friction coefficient [2]. For frictional aggregates, in the residual state, Z_c^* is less important but increases from 3.5 to 5.5 with η. Interestingly, we see also that, both in the isostatic and residual state, Z remains nearly constant for $\eta > 0$. In others words, the effect of increasing nonconvexity is therefore expressed by an increasing number of multiple contacts with the same average number of neighboring aggregates and thus for large η, the packings are loose but well connected. Figure 4(b) displays the proportion of each contact type in the residual state as a function of η. By definition, all contacts are simple at $\eta = 0$. We see that the fraction of simple contacts declines as η increases and that of multiple contacts increases at the same time. We see also that, for $\eta > 0.4$ the proportion of each contact type remains constant with η. The increasing connectivity of the particles is obviously correlated with the increase of shear strength. This is well illustrated in Fig. 5(a) which shows a map of radial forces $f_{n'} = \boldsymbol{F}\boldsymbol{n'}$, where $\boldsymbol{F}$ is the resultant of point forces acting at their contacts between two aggregates, projected along the branch vector $\boldsymbol{n'}$ (i.e. unit vector joining the centers of the two contacting aggregates). We see that stronger force chains are composed of simple contacts reinforced by double contacts, double-simple, triple and quadruple contacts.

5 FORCE TRANSMISSION AND FRICTION MOBILIZATION

The anisotropic structures seen in Fig.5(a) can be characterized more generally trough the angular dependence $\langle f_{n'}\rangle(\Omega)$ and $\langle f_{t'}\rangle(\Omega)$ of radial and orthoradial forces along the direction $\boldsymbol{n'}$, where $f_{t'}\boldsymbol{t'} = \boldsymbol{F} - f_{n'}\boldsymbol{n'}$, and $\Omega = (\theta, \phi)$ the azimutal and radial angles that define the orientations of $\boldsymbol{n'}$ in 3D. We can show that the mean radial and orthoradial force, $\langle f_{n'}\rangle$ and $\langle f_{t'}\rangle$ are respectively given by:

$$\langle f_{n'}\rangle = \int_\Omega \langle f_{n'}\rangle(\Omega) P_\Omega(\Omega) d\Omega \qquad \text{and} \qquad \langle f_{t'}\rangle = \int_\Omega \langle f_{t'}\rangle(\Omega) P_\Omega(\Omega) d\Omega, \tag{1}$$

where, $d\Omega$ is the solid angle and $P_\Omega(\Omega)$ the angular distribution of the branch vector. Note that due to quasi-static shearing, we have $\langle f_{t'}\rangle = 0$. This means that $\langle f_{t'}\rangle(\Omega)$ and $P_\Omega(\Omega)$ are orthonormal. Under the axisymmetric conditions of our simulations, these angular distributions are independent of ϕ, so that, at leading order on the spherical harmonic basis, we have [4, 9]:

$$\left\{ \begin{array}{lll} \text{(a)} \quad P_\theta(\theta) & = & \frac{1}{4\pi}\{1 + a'_c[3\cos^2(\theta - \theta_c) - 1]\}, \\ \text{(b)} \quad \langle f_{n'}\rangle(\theta) & = & \langle f_{n'}\rangle\{1 + a_{fn'}[3\cos^2(\theta - \theta_{fn}) - 1]\}, \\ \text{(c)} \quad \langle f_{t'}\rangle(\theta) & = & \langle f_{n'}\rangle a_{ft'} \sin 2(\theta - \theta_{ft}), \end{array} \right. \tag{2}$$

where, a'_c, $a_{fn'}$ and $a_{ft'}$ are the branch, radial and orthoradial force anisotropy parameters, and $\theta_c = \theta_{fn'} = \theta_{ft'} = \theta_\sigma$ the privileged directions of the corresponding angular direction coinciding with the principal direction of the shear stress. These anisotropies are interesting descriptors of granular microstructure and force transmission properties, because they underlie the different microscopic origins of shear strength. Indeed, it can be shown that the general expression of the stress tensor leads to the following simple relation [4, 9]:

$$\frac{q}{p} \simeq 0.4(a'_c + a_{fn'} + a_{ft'}), \tag{3}$$

where the cross products between the anisotropy parameters have been neglected. Figure 2(a) shows that Eq. 3 holds well for all values of η.

Figure 5(b) shows the variation of all anisotropies averaged in the steady state as a function of η. We see that a'_c and $a_{fn'}$ increases from 0.2 to 0.3 and to 0.2 to 0.4, respectively, but they saturate for $\eta > 0.3$. The saturation of a'_c is correlated with the fact that the mean number of neighbors per particle remains nearly constant with η. The large amplitude of $a_{fn'}$ reflects the fact that stronger forces chains are developed due to the increase of multiple contacts with η. Nevertheless, as shown in Sec. 4, at larger η the proportion of multiple contact remains constant and thus $a_{fn'}$ saturate also.

In contrast, we see that $a_{ft'}$ increases rapidly with η from 0.05 for $\eta = 0$ to be nearly equal to a'_c for $\eta = 0.7$. Remarking that, at the contact scale the ratio $|f_t|/(\mu f_n) \in [0, 1]$, where f_n and f_t are the normal and tangential forces, provides a good measure of the degree of the mobilization of friction, Eq. 2(c) can thus be seen as the angular mobilization

of friction in the neighbor frame [9, 12]. Indeed, it is easy to see that the mean mobilization of friction is simply given by $\langle |f_{t'}| \rangle / \langle f_{n'} \rangle = 5a_{ft'}/2$. In other words, the increase of $a_{ft'}$ underlies an increase of the friction mobilization. In fact, with η much more contacts are interlocked which have to effect to freeze the relative motion of the particles, and thus to increase the proportion of sliding particles.

6 DISCUSSION AND CONCLUSION

In this paper, we applied the contact dynamics method to simulate large samples of nonconvex aggregates. A single parameter was defined to characterize shape nonconvexity and it was varied in order to investigate its effect on the shear strength, solid fraction, texture and force transmission. It was shown that the shear strength increases with nonconvexity. By distinguishing the contact network from the neighbor network we have shown that the origins of this increase result from the increase of multiple contacts between aggregate. This leads to an increase of the proportion of interlocked aggregates. As the consequence the increasing mobilization of friction force and the associated anisotropy are key effects of non-convexity

In this article, we have developed the texture and force transmission in terms of the neighbor orientation. It will be instructive to reinterpret and to compare this result as a function of the contacts orientation. Much more work is needed in order to understand the mechanical role of each contact type on the stress transmission. An idea is to isolate the contribution of each contact on the texture and forces anisotropies. This investigation is presently underway and will be presented in a forthcoming publication.

REFERENCES

[1] Moreau, J.-J,. Geometric origin of mechanical properties of granular materials. *Eur. J. Mech. A/Solids.* (1994) **13**:93-114.

[2] Roux, J.-N,. Some numerical methods in multibody dynamics: application to granular materials. *Phys. Rev. E.* (2000) **61**: 6802-6836.

[3] Mirghasemi, A., Rothenburg, L., and Maryas, E. Influence of particle shape on engineering properties of assemblies of two-dimensional polygon-shaped particles. *Geotechnique.* (2002) **3**:209.

[4] Ouadfel, H., Rothenburg, L. 'Stress-force-fabric' relationship for assemblies of ellipsoids. *Mechanics of Materials.* (2001) **33**:201-221.

[5] Donev, A., Stillinger, F., Chaikin, P. and Torquato, S. Unusually Dense Crystal Packings of Ellipsoids. *Phys. Rev. Lett.* (2004) **92**: 255506.

[6] Nezami, E.G., Hashash, Y.M.A., Zhao, D. and Ghaboussi, J. A fast contact detection algorithm for 3-D discrete element method. *Computers and Geotechnics* (2004) **31**: 575-587.

[7] Mitchell, J.K., Soga, K. *Fundamentals of Soil Behavior*. Wiley, New York (2005).

[8] Azéma, E., Radjai, F., Peyroux, R. and Saussine, G. Force transmission in packing of pentagonal particles. *Phys. Rev. E.* (2007) **76**:011301.

[9] Azéma, E., Radjai, and Saussine, G. Quasistatic rheology, force transmission and fabric properties of a packing of irregular polyhedral particles. *Mechanics of Materials* (2009) **41**:729-741.

[10] Radjai, F. and Richefeu, V., Contact dynamics as a nonsmooth discrete element method *Mechanics of Materials* (2009) **41**: 715-728

[11] Azéma, E. and Radjai, F., Stress-strain behavior and geometrical properties of packings of elongated particles. *Phys. Rev. E.* (2010) **81**: 051304.

[12] Saint-Cyr, B., Delenne, J.-Y., Voivret C., Radjai, F. and Sornay, P. Rheology of granular materials composed of nonconvex particles. *Phys. Rev. E.* (2010) Submited.

[13] For our simulations, we used the LMGC90 which is a multipurpose software developed in Montpellier, capable of modeling a collection of deformable or undeformable particles of various shapes (spherical, polyhedral, or polygonal, and non-convex) by different algorithms.